Modulated rotating orthogonal polarization parametric imaging, a preliminary study

Bozhi Liu[1,3][0000-0002-2157-5597], Jichuan Xiong[1,3][0000-0002-7051-802X], Juan Liu[1][0000-0003-2981-8255], Heng Zhang[1][0000-0003-4740-0338], Bin Xu[1][0000-0001-7275-3480], Lianping Hou[2][0000-0001-8405-8389], John H. Marsh[2][0000-0002-2851-413X] and Xuefeng Liu[1,*][0000-0003-0568-5144]

[1] School of Electronic and Optical Engineering, Nanjing University of Science and Technology, 200 Xiaolingwei, Nanjing, 210094, China
[2] James Watt School of Engineering, University of Glasgow, Glasgow, G12 8QQ, UK
[3] These authors contributed equally to this work
liuxf_1956@sina.com

Abstract. We propose a new microscopic imaging technique in which the polarization angles of illumination light and a polarizer in front of the imaging sensor oriented orthogonally to the illumination polarization are rotated synchronously. A series of images of cervical cells was recorded under different illumination polarization angles and an algorithm was used to fit the pixel intensity variations of the images. A reconstruction method was employed to map the anisotropic properties of cervical cells in the form of a set of polarization parameters. Analysis of the images of the cervical cells and comparison with traditional methods indicate that this technique provides higher contrast and sensitivity.

Keywords: Orthogonal polarization, Polarization parameter, Cervical cell.

1 Introduction

Orthogonal polarization imaging is a useful method for imaging superficial tissues such as microcirculation [1,2]. Orthogonal polarization imaging uses linearly polarized light to illuminate the tissue and captures images through a linear polarizer that is oriented in the orthogonal polarization state. It prevents surface-reflected light and polarization-maintaining light from contributing to the recorded image [1-4]. This method can create high-contrast microvascular images and can be implemented in a small optical probe for clinical diagnosis. An improved technique called rotating orthogonal polarization difference imaging was subsequently introduced [5]. In this technique an orthogonal polarization image is captured and then the angles of the two polarizers are exchanged to obtain a second image. The images are processed to give a normalized orthogonal polarization difference image [(first-second) / (first + second)] that is free from surface reflection and sensitive to the polarization properties of the underlying tissue. This technique has been applied to image the tendon and results indicate that it has potential for analyzing the alignment of collagen. However, this approach does not provide direct

quantification of the polarization properties. It has been found that modulating the polarization in the imaging system is usually beneficial in extracting quantitative parameters [6-9].

In this paper, we present a new technique, namely modulated rotating orthogonal polarization parametric imaging, which utilizes the advantages of orthogonal polarization imaging and polarization modulation to generate higher contrast and signal-to-noise ratio images that can be used to quantify the polarization properties of a sample. The technique is based on a conventional orthogonal polarization imaging system but the illumination and detection polarization angles are rotated synchronously in defined steps over a range of 180 degrees. Each corresponding pixel of the images recorded under different angles is fitted to an analytical function based on the Jones matrix to reconstruct a set of polarization parametric images. Experiments on cervical cells have been conducted and the results show that this technique can improve the contrast and resolution. This suggests that it is useful for characterizing superficial tissues in clinical diagnosis.

2 Experiment Setup and Data Processing

The system uses a conventional microscopic light path (Olympus BX51) with additional motorized rotating polarizers. The polarization of the incident light is modulated accurately with a rotating polarizer and reflected light from the sample is filtered through another synchronously rotating polarizer which is oriented orthogonally to the illumination polarizer. The motors and CCD camera are controlled by a computer, so the polarizers are rotated and images are recorded automatically during the process of image acquisition.

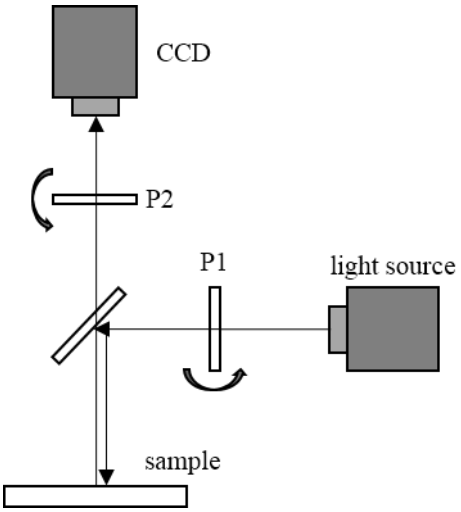

Fig. 1. Schematic of the experimental setup

As shown in Fig. 1, illumination light with a central wavelength of 532 nm is propagated through a linear polarizer P1, reflected by a beam-splitter and used to illuminate the sample. Surface reflected or polarization-maintaining light is rejected while multiple-scattered light passes through the linear polarizer that is always oriented in the orthogonal polarization state. Two orthogonally oriented linear polarizers P1 and P2 are driven by motors to rotate synchronously in angular steps of (π/N) and then the CCD camera (Basler acA2040-35gm) records an image for each step. The image size is 2448×2050 pixels and each pixel represents an area of 3.45 μm × 3.45 μm. The process is repeated n times over a range of π radians and N images are recorded.

First, consider the linear birefringence. When the two polarizers are rotated continuously, the intensity of the output light changes periodically. The Jones matrix of the elements in the optical path can be written as,

$$E_{out} = G_{P2} G_S G_{P1} E_{in} \tag{1}$$

$$G_{P1} E_{in} = \begin{pmatrix} \cos\theta \\ \sin\theta \end{pmatrix} \tag{2}$$

$$G_S = \begin{pmatrix} \cos\varphi & -\sin\varphi \\ \sin\varphi & \cos\varphi \end{pmatrix} \begin{pmatrix} 1 & 0 \\ 0 & e^{i\delta} \end{pmatrix} \begin{pmatrix} \cos\varphi & \sin\varphi \\ -\sin\varphi & \cos\varphi \end{pmatrix} \tag{3}$$

$$G_{P2} = \begin{pmatrix} \cos^2\left(\theta+\frac{\pi}{2}\right) & \frac{1}{2}\sin\left[2\left(\theta+\frac{\pi}{2}\right)\right] \\ \frac{1}{2}\sin\left[2\left(\theta+\frac{\pi}{2}\right)\right] & \sin^2\left(\theta+\frac{\pi}{2}\right) \end{pmatrix} \tag{4}$$

where θ is the angle of the polarizer P1. The sample is treated as a waveplate with δ as the phase retardance between the x and y components and φ as the rotation angle of the polarization ellipse. G_{P1}, G_{P2}, and G_{sample} are the Jones matrices of the polarizer P1, P2 and the sample respectively. E_{in} and E_{out} are the electric fields of light from the source and that incident on the CCD.

The intensity of the light incident on the CCD can be expressed as

$$I = E_{out} E_{out}^{*} = \frac{1}{2}\sin^2\left(\frac{\delta}{2}\right)\left(1-\cos 4\varphi\cos 4\theta - \sin 4\varphi\sin 4\theta\right) \tag{5}$$

For the recorded images at certain limited number of angles θ_i in the experiment, the intensity also follows the expression in Eq. 6, only the variation is discrete,

$$I_i = k_0 + k_1\cos 4\theta_i + k_2\sin 4\theta_i \tag{6}$$

$$k_0 = \frac{1}{2}\sin^2\left(\frac{\delta}{2}\right),\ \ k_1 = -\frac{1}{2}\sin^2\left(\frac{\delta}{2}\right)\cos 4\varphi,\ \ k_2 = -\frac{1}{2}\sin^2\left(\frac{\delta}{2}\right)\sin 4\varphi \tag{7}$$

Second, consider the dichroism. The difference of absorptivity in different polarization directions introduces a component,

$$I_{D_i} = D\cos\left(2\left(\theta_i - \varphi_D\right)\right) = k_3\cos 2\theta_i + k_4\sin 2\theta_i \tag{8}$$

Here, φ_D represents the orientation of the dichroism, which means that the absorptivity is the lowest in this direction.

Finally, the intensity should follow the expression in Eq. 9,

$$I_i = k_0 + k_1\cos 4\theta_i + k_2\sin 4\theta_i + k_3\cos 2\theta_i + k_4\sin 2\theta_i \tag{9}$$

The coefficients k_i are calculated from

$$\begin{aligned} &k_0 = \sum_1^N I_i\frac{1}{N},\ \ k_1 = \sum_1^N I_i\frac{2}{N}\cos 4\theta_i,\ \ k_2 = \sum_1^N I_i\frac{2}{N}\sin 4\theta_i, \\ &k_3 = \sum_1^N I_i\frac{2}{N}\cos 2\theta_i,\ \ k_4 = \sum_1^N I_i\frac{2}{N}\sin 2\theta_i \end{aligned} \tag{10}$$

then the polarization parameters of the sample are calculated from

$$\cos\delta = 1 - 4k_0,\ \ \varphi = \frac{1}{4}\tan^{-1}\left(\frac{k_2}{k_1}\right),\ \ \varphi_D = \frac{1}{2}\tan^{-1}\left(\frac{k_4}{k_3}\right) \tag{11}$$

Expressions for calculating these parameters are retained in each of the corresponding pixels of the CCD and a series of parametric images can be formed with them, enables the polarization properties of the sample to be quantified.

During the measurement, the recorded images were first normalized before reconstruction. A new image $I_i'(x,y)$ was calculated for each recorded raw image $I_i(x,y)$,

$$I_i'\left(x,y\right) = \frac{I_i\left(x,y\right)}{\frac{2}{N}\sum_1^N I_i\left(x,y\right)} \tag{12}$$

This technique is compatible with the conventional orthogonal polarization imaging method because the recorded images at each rotation angle of the polarizers are equivalent to those of orthogonal polarization images, while any two pairs of images at different rotation angles θ and θ +90° taken by this method can be used to create results of orthogonal polarization difference imaging.

3 Results and discussion

As shown in Fig. 2, in reflection images using a conventional microscope, we can only observe the surface shape of the cervical cell because of the cell membrane. The inner

structures, such as the endoplasmic reticulum composed of cytoplasm distributed outside the nucleus, can only observed in transmission imaging results as stripe net patterns. Also, it is difficult to observe the structure of the nucleus in either transmission or reflection.

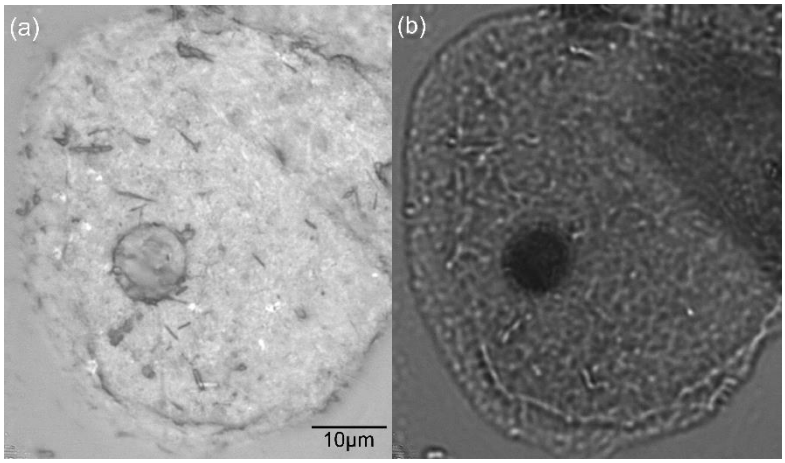

Fig. 2. (a) Reflection imaging results and (b) transmission imaging results by conventional microscope. Scale bar, 10 μm.

The polarization parameter images $\cos\delta$, φ and φ_D of the same cervical cell were taken using the system described in Fig. 1. In this experiment, a 100× objective was used and 12 images were recorded ($N = 12, \Delta\theta = 15°$). The polarization parameter images $\cos\delta$, φ are shown in Fig. 3. For comparison, the polarization parameter images φ_D and orthogonal polarization difference image processed from the same set of raw data are shown in Fig. 4. They are all significantly different from reflection imaging results by conventional microscope.

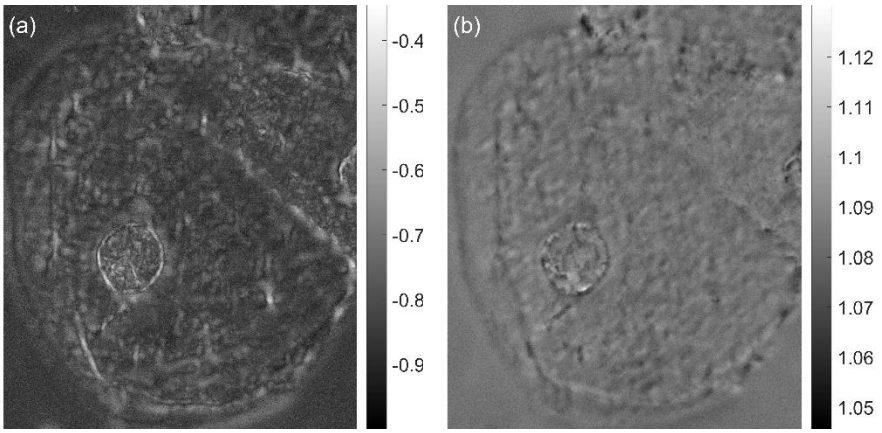

Fig. 3. (a) The polarization parameter image of cos δ; (b) the polarization parameter image of φ. Color bar, the range of value of different polarization parameters.

Figures 3 (a) and (b) are the polarization parameter images cos δ and φ, which are free from surface reflections and sensitive to the polarization properties of the sample. The cos δ parametric image provides more detail of the anisotropic optical property inside the cell with patterns corresponding to details of the endoplasmic reticulum in the transmission imaging result, which can help in determining the distribution of the cytoplasm in the cell. The edges of the nucleus in the cos δ parametric images are sharper than in other images, i.e. φ in Fig. 3 (b) and conventional microscope images in Fig. 2, because the cos δ parameter image is not affected by initial polarization direction of the polarizers; photons back-scattered by nucleolemma are mainly collected and lead to different optical phase retardance from nearby areas.

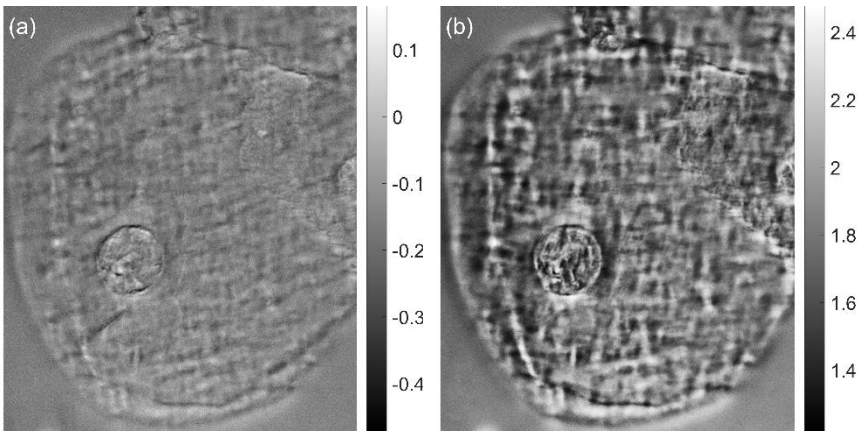

Fig. 4. (a) The orthogonal polarization difference image; (b) the polarization parameter images of φ_D. Color bar, the range of value of different polarization parameters.

Fig. 4 (a) is the orthogonal polarization difference image, which was calculated from the first and seventh images ($\Delta\theta = 90°$), i.e. $[(I_1 - I_7)/(I_1 + I_7)]$. Fig. 4 (b) is the φ_D parametric image, which is similar to Fig. 4 (a), demonstrating that the φ_D parametric images also correspond to dichroism [5]. However, the initial polarization state of the polarizers will affect the orthogonal polarization difference image greatly, as the results for different initial states are quite different. In our method, all the recorded images are used in the calculation; as is shown in Fig. 5, the phase of the component in the light intensity curve caused by dichroism of the sample is used to determine the orientation of the dichroism. Compared with the orthogonal polarization difference image which only uses two images with random initial states, the influence of the initial polarization direction of polarizer on the φ_D parameter image is far smaller. Besides, the φ_D parameter image has higher contrast and lower noise. The φ_D parameter image is believed to be related to the alignment of the fibrous structure, which can be used to map endoplasmic reticulum composed of cytoplasm inside the cell [5, 10].

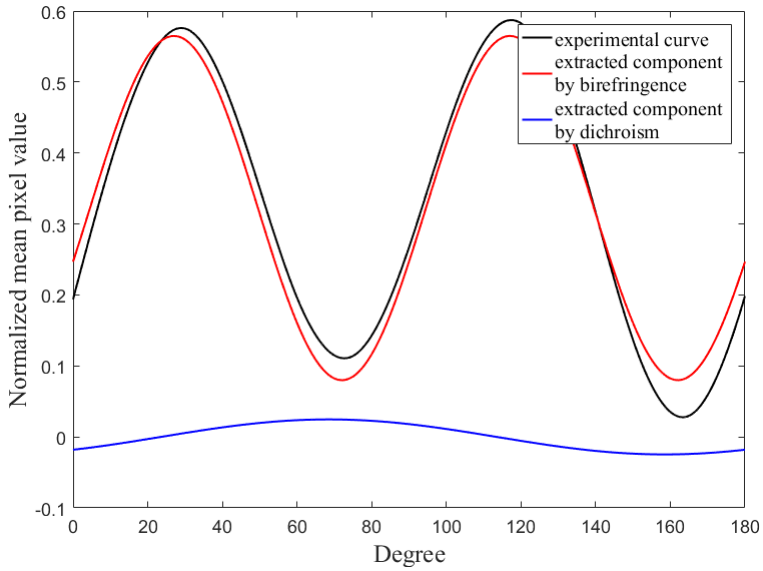

Fig. 5. The curves of normalized mean pixel value of raw images, and separated components caused by birefringence and dichroism which are used to calculate different polarization parameters

The nucleus areas of the cells are compared in Fig. 6, using different imaging methods. In general, modulated rotating orthogonal polarization parametric imaging has significant advantages over traditional methods. This is due to the elimination of surface-reflections by the orthogonal polarizers and the polarization properties that are recovered as a result of rotating the modulation of the illumination polarization states.

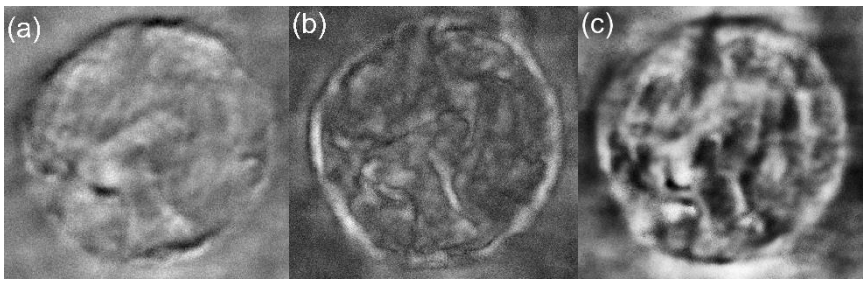

Fig. 6. (a) Orthogonal polarization difference image (b) $\cos\delta$ parametric image and (c) φ_D parametric image of the nucleus, respectively.

4 Conclusion

We have developed a modulated orthogonal polarization parametric imaging technique. A function was derived to describe the variation in pixel intensity when synchronously rotating two orthogonal polarizers in the illumination and imaging optical path. By fitting each corresponding pixel of the images, a set of polarization parametric images of cervical cells was obtained. The polarization properties of the cervical cell can be retrieved from the $\cos\delta$, φ and φ_D parametric images, which quantify the phase retardance, rotation of polarization ellipse and the orientation of dichroism by the sample. The results show that the proposed method achieves higher contrast and sensitivity than conventional orthogonal polarization imaging. In future work, the performance of this method will be investigated comprehensively and utilized for imaging other cells and tissues.

Acknowledgement

This work was supported by the National Key Scientific Instruments and Equipment Development Project under Grant No.61827814, Natural Science Foundation of Beijing Municipality under Grant No. Z190018, the Fundamental Research Funds for the Central Universities under Grant No.30920010011 the Postdoctoral Foundation of Jiangsu Province under Grant No. 2020Z331, and the Ministry of Education collaborative project B17023. The authors would like to acknowledge support from the UK Engineering and Physical Sciences Research Council (Grant EP/R042578/1).

References

1. W. Groner, J. W. Winkelman, A. G. Harris, C. Ince, G. J. Bouma, K. Messmer, and R. G. J. N. m. Nadeau, "Orthogonal polarization spectral imaging: a new method for study of the microcirculation," Nature Medicine **5**, 1209-1212 (1999).
2. V. Černý, Z. Turek, and R. J. P. R. Pařízková, "Orthogonal polarization spectral imaging," Physiological Research **56**, 141-147 (2007).
3. S. P. Morgan and I. M. J. O. l. Stockford, "Surface-reflection elimination in polarization imaging of superficial tissue," Optics Letters **28**, 114-116 (2003).
4. Q. Zhu, I. M. Stockford, J. A. Crowe, and S. P. J. J. o. b. o. Morgan, "Experimental and theoretical evaluation of rotating orthogonal polarization imaging," Journal of Biomedical Optics **14**, 034006 (2009).
5. S. P. Morgan, Q. Zhu, I. M. Stockford, and J. A. J. O. l. Crowe, "Rotating orthogonal polarization imaging," Optics Letters **33**, 1503-1505 (2008).
6. R. J. C. S. H. P. Oldenbourg, "Polarized light microscopy: principles and practice," Cold Spring Harbor Protocols **2013**, pdb. top078600 (2013).
7. W. Kaminsky, K. Claborn, and B. J. C. S. R. Kahr, "Polarimetric imaging of crystals," Chemical Society Reviews **33**, 514-525 (2004).
8. R. Liao, N. Zeng, X. Jiang, D. Li, T. Yun, Y. He, and H. J. J. o. B. O. Ma, "Rotating linear polarization imaging technique for anisotropic tissues," Journal of Biomedical Optics 15, 036014 (2010).

9. K. Ullah, X. Liu, M. Habib, and Z. J. A. P. Shen, "Subwavelength far field imaging of nanoparticles with parametric indirect microscopic imaging," ACS Photonics **5**, 1388-1397 (2018).
10. D. Beach, C. Bustamante, K. Wells, and K. J. B. j. Foucar, "Differential polarization imaging. III. Theory confirmation. Patterns of polymerization of hemoglobin S in red blood sickle cells," Biophysical Journal **52**, 947-954 (1987).